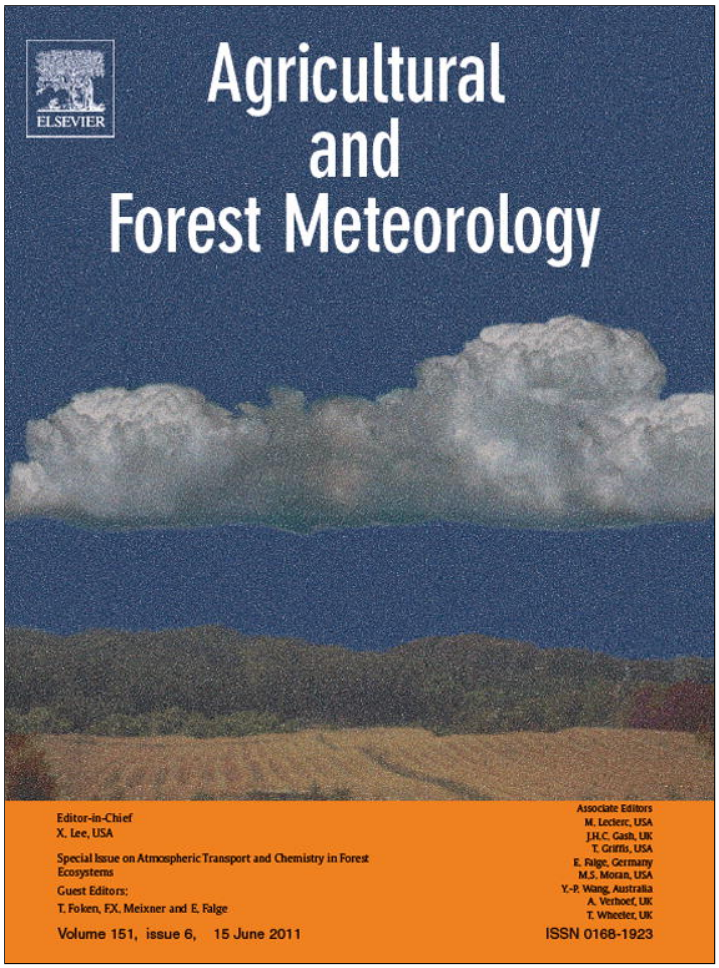

Agricultural and Forest Meteorology 151 (2011) 645–654

Contents lists available at ScienceDirect

Agricultural and Forest Meteorology

journal homepage: www.elsevier.com/locate/agrformet

Measured deuterium in water vapour concentration does not improve the constraint on the partitioning of evapotranspiration in a tall forest canopy, as estimated using a soil vegetation atmosphere transfer model

Vanessa Haverd [a,b,*], Matthias Cuntz [c,d,e], David Griffith [b], Claudia Keitel [c,f], Carol Tadros [g], John Twining [g]

[a] CSIRO Marine and Atmospheric Research, GPO Box 3023, Canberra, ACT 2601, Australia
[b] Department of Chemistry, University of Wollongong, NSW 2522, Australia
[c] Environmental Biology Group, Research School of Biology, GPO Box 475, Canberra, ACT 2601, Australia
[d] Max-Planck-Institut für Biogeochemie, Hans-Knöll-Str. 10, 07745 Jena, Germany
[e] UFZ – Helmholtz Centre for Environmental Research, Permoserstr. 15, 04318 Leipzig, Germany
[f] Faculty of Agriculture, Food & Natural Resources, University of Sydney, Eveleigh, NSW 2015, Australia
[g] Institute for Environmental Research, Australian Nuclear Science and Technology Organisation (ANSTO), Menai, NSW 2234, Australia

ARTICLE INFO

Article history:
Received 20 April 2010
Received in revised form 27 January 2011
Accepted 7 February 2011

Keywords:
Deuterium
Water vapour
Evapotranspiration
Soil evaporation
Transpiration
Atmospheric dispersion
Lagrangian time scale
Turbulent transport in plant canopies

ABSTRACT

Partitioning the evapotanspiration (*ET*) flux in a forest into its component fluxes is important for understanding the water and carbon budgets of the ecosystem. We use non-linear parameter estimation to determine the vertical profile of the Lagrangian timescale (T_L) and partitioning of *ET* that simultaneously optimise agreement between modelled and measured vertical profiles of temperature, water vapour, carbon dioxide concentrations, and deuterated water vapour for a two-week period in November 2006. High precision real-time trace gas measurements were obtained by FTIR spectroscopy. Modelled temperature and concentration profiles are generated using a Lagrangian dispersion theory combined with source/sink distributions of HDO, H_2O, sensible heat, and CO_2. These distributions are derived from an isotopically enabled multilayer Soil Vegetation Atmospheric Transfer (SVAT) model subject to multiple constraints. The soil component of the model was tested in isolation using measured deuterium content of soil chamber evaporate, while the leaf component was tested using isotopic analyses of leaf and xylem water, combined with leaf-level gas exchange measurements. Optimisation of T_L and the partition of *ET* was performed twice: once using only temperature, H_2O and CO_2 profiles and a second time including HDO as well. The modelled vertical concentration profiles resulting from inclusion of HDO in the cost function demonstrate our ability to make consistent estimates of both the scalar source distributions and the deuterium content of the water vapour sources. However, introducing measurements of deuterium in water vapour does not significantly alter resulting estimates of normalised T_L (0.4 ± 0.1 at canopy top) and the partition of *ET* ($85 \pm 2\%$ transpiration), suggesting that the additional data and modelling required to use deuterium are not warranted for the purpose of partitioning *ET* using the framework presented here.

1. Introduction

Understanding the strong coupling between water and carbon fluxes in ecosystems requires a detailed understanding of the individual component fluxes. For water, transpiration (*T*) and evaporation (*E*) can be separated with different combinations of lysimeters, porometers, Bowen ratio, eddy-covariance, and sap flow measurements. All these methods bear large uncertainties (e.g. Herbst et al., 1996). Using observations of the stable isotopic composition of water vapour exchanged between vegetation and the atmosphere in conjunction with the classical methods above can potentially reduce associated errors (e.g. Williams et al., 2004). This is because the isotopic composition of the water in the individual components can be quite distinct and the fluxes are therefore isotopically tagged. However, most isotope-based separations of transpiration and evaporation do assume isotopic steady-states in soil and vegetation (Ferretti et al., 2003; Moreira et al., 1997; Williams et al., 2004; Xu et al., 2008; Yakir and Wang, 1996; Yepez et al., 2005). This assumption neglects significant isotopic gradients from stomata to xylem and within the soil column (e.g. Allison and Barnes, 1983; Farquhar et al., 1993; Yakir and Sternberg, 2000),

* Corresponding author at: CSIRO Marine and Atmospheric Research, GPO Box 3023, Canberra, ACT 2601, Australia. Tel.: +61 2 6246 5981; fax: +61 2 6246 5988.
E-mail address: Vanessa.Haverd@csiro.au (V. Haverd).

0168-1923/$ – see front matter.
doi:10.1016/j.agrformet.2011.02.005

potentially leading to biases in the isotope-derived component fluxes.

In the previous work (Haverd et al., 2009) (hereafter Hav09), we simultaneously estimated the partitioning of evapotranspiration (*ET*) between ground and canopy, together with the turbulent Lagrangian timescale (T_L) in a 40 m tall Eucalyptus forest in south-eastern Australia for a two-week campaign period. This was done by optimising modelled vertical scalar concentration profiles (potential temperature (θ), water vapour and CO_2) against corresponding measurements. Inputs to the predicted profiles were source/sink distributions from a Soil Vegetation Atmosphere Transfer (SVAT) model, and vertical profiles of the turbulence statistics, namely the standard deviation of the vertical wind velocity (σ_w) and T_L. Of these, the largest uncertainties were in the ground/canopy partitions of sensible and latent heat fluxes, and hence the evapotranspiration partition between ground and canopy, and in T_L. SVAT model predictions of net fluxes of CO_2, water vapour and sensible heat were well constrained by measured fluxes above the canopy, the ground/canopy partition of CO_2 was well-constrained by 2 independent sets of ground chamber measurements, and σ_w was measured. Therefore two parameters specifying the vertical profile of T_L and one parameter for modifying the SVAT model predictions of the ground/canopy sensible and latent heat flux partitions were optimised. This led to agreement between observed and predicted concentrations to within the 95% confidence limits for most of the hourly mean profiles, and to revised estimates of T_L and ground/canopy partitions of sensible and latent heat fluxes.

In the current work, we build on the analysis in Hav09 by including vertical profiles of deuterium isotopic content (δD) in water vapour in addition to those of potential temperature, water vapour and CO_2 concentrations, which were used previously. δD is defined as:

$$\delta D = \frac{[HDO]_{sample}/[H_2O]_{sample}}{[HDO]_{ref}/[H_2O]_{ref}} - 1 \quad (1)$$

where the reference material is V-SMOW (Gonfiantini, 1978). The objective is to use δD to provide an additional constraint on the estimates of T_L and ground/canopy partitions of sensible and latent heat fluxes. This extension requires measured vertical profiles of δD in atmospheric water vapour and an isotopically enabled SVAT model, capable of prediciting δD in the soil evaporate and transpirate.

In Section 2, we describe our approach for simultaneously constraining estimates of T_L and the partition of evapotranspiration. Section 3 describes the field measurements. In Section 4 we describe the isotopically enabled SVAT model, including its validation against measurements of δD in leaf water and soil evaporate within a chamber. We also present predictions from the validated model of the CO_2, sensible heat and latent heat sources and δD in *ET* for the ground and canopy. In Section 5, we compare predicted and observed vertical concentration profiles and evaluate the additional constraint provided by δD profiles on our final estimates of T_L and the ground/canopy partition of *ET*.

2. Approach to using vertical concentration profiles to constrain the ground/canopy partition of *ET* and the turbulent Lagrangian time scale

The relationship between the vertical distribution of scalar source/sinks and scalar concentrations within plant canopies may be written:

$$c_i - c_{ref} = \sum_{j=1}^{m} D_{ij} S_j \Delta z_j \quad (2)$$

in which c_i and c_{ref} are the concentration at height above the ground z_i, and at a reference height (z_{ref}, typically above the canopy), S_j is the source/sink strength at height j distributed across a layer of thickness Δz_j, and D_{ij} are the elements of the dispersion matrix relating c_i to S_j.

Eq. (2) requires *D* and *S*. In order to use it to estimate parameters specifying the partition of *ET* and T_L, we require: (i) *D* as a function of T_L, and a parametric form of the vertical profile of T_L within the canopy; (ii) specification of *S*, and a parameter which can be used to correct the prior estimate of the ground/canopy partitions of sensible and latent heat fluxes and hence of *ET*; (iii) specification of the parameter estimation procedure, including the search strategy and formulation of the cost function to be minimised. Below we discuss how these requirements are met.

2.1. In-canopy dispersion

Calculation of the dispersion matrix *D* requires knowledge of σ_w, the vertical profile of the standard deviation of vertical velocity, and T_L, the Lagrangian time scale. We adopt the widely used Localised Near-Field (LNF) theory of Raupach (1989a,b), and restrict our analysis to times when this theory applies (i.e. periods of fully coupled flow: see Section 3.1). The concentration in Eq. (2) is expressed as the sum of near-field and far-field components ($c_i = c_{ni} + c_{fi}$). The diffusive far-field component, c_{fi}, provides large-scale variation in the concentration profile, upon which is superimposed detailed local structure due to c_{ni}, the non-diffusive near-field component. The dependences of the near- and far-field concentration components (and hence *D*) on σ_w and T_L are as follows.

The continuous forms of the near- and far-field concentration components depend on σ_w and T_L as:

$$c_n(z) = \int_0^{\infty} \frac{S(z_s)}{\sigma_w(z_s)} \left\{ k_n \left[\frac{z - z_S}{\sigma_w(z_s) T_L(z_s)} \right] + k_n \left[\frac{z + z_S}{\sigma_w(z_s) T_L(z_s)} \right] \right\} dz_S \quad (3)$$

$$c_f(z) = c_f(z_{ref}) + \int_z^{z_{ref}} \frac{F(z')}{K_f(z')} dz' \quad (4)$$

In Eqs. (3) and (4), z_s is the source height; z_{ref} is an arbitrary reference height, k_n is a 'near-field kernel' approximated by: $k_n(\varsigma) = -0.3989 \ln(1 - e^{-|\varsigma|}) - 0.1562 e^{-|\varsigma|}$; $c_f(z_{ref}) = c(z_{ref}) - c_n(z_{ref})$; $F(z)$ is the flux density, related to the source strength by $F(z) = \int_0^z S(z')dz'$ and to the far-field concentration by the gradient diffusion relationship $F(z) = -K_f(z)(dc_f/dz)$, where K_f is the far-field diffusivity, $K_f(z) = \sigma_w{}^2(z) T_L(z)$.

To calculate the elements D_{ij} we follow Raupach (1989a). Consider a scalar that is released uniformly in layer j with source strength, S_j, but with zero strength in all other layers. The resulting partial concentration profile c_i defines the elements of the dispersion matrix for dispersion from layer j to concentration at height z_i, i.e.

$$D_{ij} = \frac{c_i - c_R}{S_j \Delta z_j} \quad (5)$$

Each element of D_{ij} has a near field and a far field component because $c_i = c_{ni} + c_{fi}$.

We assume a unit source strength in each layer and use Eqs. (3) and (4) to estimate c_{ni} and c_{fi} and hence the coefficients D_{ij} from Eq. (5), provided we know $\sigma_w(z)$ and $T_L(z)$.

While $\sigma_w(z)$ is measurable, the vertical profile of T_L is not. Our prior estimate of the T_L profile is a fit of Eq. (6) (Styles et al., 2002):

$$\frac{T_L(z) u_*}{h_c} = c_2 \frac{1 - \exp(-c_1 z/h_c)}{1 - \exp(-c_1)} \quad (6)$$

to the single-point estimate of the Eulerian time scale (T_E):

$$T_L = \frac{\beta \bar{u} T_E}{\sigma_w} \tag{7}$$

with

$$T_E = \int_0^\infty \frac{w'(t)w'(t+\tau)}{\sigma_w^2} d\tau \tag{8}$$

where $w' = w - \bar{w}$ is the instantaneous deviation of the vertical wind velocity, w, from its time-averaged value, $\bar{w}$. $\bar{u}$ is the mean horizontal wind speed and β is a constant of order 1 (Raupach, 1989a). As in Hav09, we set β to 1 and obtained the velocity statistics from a vertical array of 3D sonic anemometers.

2.2. Source/sink distributions

We use an isotopically enabled SVAT model to estimate the vertical source/sink distributions of CO_2, sensible heat, water vapour (H_2O) and deuterated water vapour (HDO). The predicted net fluxes of CO_2, sensible heat and H_2O are constrained by measurements of these quantities above the canopy, and the ground source of CO_2 is constrained by chamber measurements. Unlike CO_2, the ground sources of water vapour and sensible heat are not measured. Therefore we treat the SVAT modelled ground/canopy partitions of these quantities as prior estimates and introduce a partition correction parameter, $x_{\lambda E}$. The corrected latent heat flux (λE) at the soil is set to $(1 + x_{\lambda E})\lambda E^0_{\mathrm{soil}}$ where $\lambda E^0_{\mathrm{soil}}$ is the SVAT model output value, and the prior estimate of $x_{\lambda E}$ is zero. In order to conserve the total heat flux at the soil surface, the sensible heat flux at the ground (H_{soil}) was set to $H^0_{soil} - x_{\lambda E}\lambda E^0_{soil}$. Also, canopy contributions to the latent and sensible heat fluxes were modified to conserve net H and λE (cf. Hav09). The same partition correction parameter was applied to prior estimates of the ground and canopy sources of HDO.

2.3. Parameter estimation

The Gauss–Levenberg–Marquardt method is used in the optimisation process, as implemented in the model-independent parameter estimation software, PEST (Doherty, 1999). The cost function to be minimised in this process is the sum of partial costs Φ_v where v refers to the atmospheric variable being fitted (θ, H_2O, CO_2, δD). The kth observation for each fitted variable is constructed as the average of $n_{v,k}$ ensemble members (see Section 3). Each partial cost function is defined in terms of a weighting, $w_{v,k}$, for each observation and a residual between the observation and prediction, $r_{v,k}$:

$$\Phi_c = \sum_{k=1}^{n_{\mathrm{obs},v}} (w_{v,k} r_{v,k})^2 \tag{9}$$

where $n_{\mathrm{obs},v}$ is the number of observations for each variable. We specify the weightings, such that each concentration type contributes equally to the prior cost, and each observation is weighted by the number of ensemble members, $n_{v,k}$, contributing to it. This leads to:

$$w_{v,k} = \sqrt{\frac{n_{v,k}/N_v}{\sum_{i=1}^{n_{\mathrm{obs},v}} n_{v,i} {r_{v,i}}^2}} \tag{10}$$

where N_v is the number of concentration types.

3. Measurements

Measurements other than those of the isotopic species are described in Hav09 and summarised briefly below. The analysis of trace gases and their isotopologues by FTIR spectroscopy is novel and is described in the appendix. We describe the new isotopic measurements in more detail: firstly the measurement of vertical profiles of δD in atmospheric water vapour, followed by the auxiliary measurements used to independently validate the leaf-level and soil components of the isotopically enabled SVAT model.

3.1. Tower measurements

Measurements were made in a 40 m tall temperate Eucalyptus forest at the Tumbarumba Ozflux site (35.6557°S, 148.1521°E, elevation 1200 m) in southeast Australia. Hourly vertical flux densities of CO_2 (F_c), latent heat (λE) and sensible heat (H) were measured continuously using the eddy covariance technique, with sensors mounted on top of a 70 m mast (Leuning et al., 2005). Profiles of air temperature were measured using unventilated, 100 μm copper-constantan thermocouples mounted beneath radiation shields on the mast. High-precision water vapour and trace gas profiles including CO_2, H_2O, CH_4, N_2O, CO and the isotopologues HDO and $^{13}CO_2$ were measured from 7 sampling heights (2.0, 4.4, 10.4, 26.3, 35.4, 43.4, 70.1 m) on the mast during a two-week campaign (13–26 November 2006), using two portable Fourier transform infrared (FTIR) spectrometers. The FTIR measurements are described in detail in the appendix. Separate instruments were used for H_2O and trace gases so that the air could be dried for more accurate CO_2 analysis. Each height of the 7-point profile was sampled by both analysers for 2 min out of each 30-min period required to analyse the entire profile. The time series of concentrations at each level were interpolated linearly in time and re-sampled at the nearest integral hour to produce quasi-instantaneous vertical profiles. Hourly ensemble mean profiles for comparison with model output were constructed by selecting times when the gradient Richardson number $Ri \leq 1.0$ at any height below 70 m, referencing the corresponding vertical concentration profiles to the value at the 40 m height (canopy top) and averaging them. The Richardson number, $Ri = (g/\bar{\theta})(\partial\bar{\theta}/\partial z)/(\partial\bar{u}/\partial z)^2$ was evaluated from mean hourly, 8-point vertical profiles of horizontal wind-speed and potential temperature, θ measured at 0.55, 4.8, 10.6, 26.0, 34.7, 42.4, 55.7 and 70.0 m. Partial derivatives were estimated by differentiating cubic spline interpolants of the profiles. The above selection criterion ensured that our analysis was restricted to periods of fully coupled flow within and above the canopy and hence that LNF theory was applicable.

Three-dimensional sonic anemometers (CSAT-3, Campbell Scientific, Logan, UT; and HS-50, Gill Instruments Ltd., Lymington, UK) were used to measure w at 8 heights (0.5, 1.9, 11.1, 18.7, 27.2, 35.0, 43.5, 70.0 m) within and above the canopy. The data from the sonic anemometers were used to calculate profiles of T_E using Eq. (8) and thence a prior estimate of T_L (Eq. (7)). CO_2 fluxes at the ground were measured using an infra-red gas analyser attached to ten automated, pneumatic open-and-close chambers (Fest et al., 2009) and found to agree well with CO_2 fluxes from the ground derived from air temperature and soil moisture data via a correlation developed from earlier static chamber measurements using absorption of CO_2 by soda lime (Keith and Wong, 2006).

3.2. Other measurements of δD in H_2O

3.2.1. Soil chamber

The soil chamber was used to obtain measurements of δD of soil evaporate in a controlled environment for the purpose of testing in isolation the soil component of the isotopically enabled SVAT model. The soil chamber consisted of a 1 m length of PVC pipe (diameter 15 cm), with one end inserted 2 cm into the soil, and an end-cap on the top. A fan was installed on the inside of the end-cap, and inlet and outlet tubes were inserted through holes in the end-cap and extended half-way down the chamber. The inlet

tube was supplied with air from a sampling point at 26.5 m on the tower, while the outlet tube was connected to a rotary pump, which flushed the chamber at a rate of 3 L min^{-1}. At two-hourly intervals, and within 10 min of the 26.5 m tower line being sampled, air from the outlet tube was sampled by the FTIR. This allowed the δD of the soil evaporate in the chamber to be computed as (Evans et al., 1986):

$$\delta D_{\mathrm{evap}} = \frac{\delta D_{\mathrm{out}} \chi_{\mathrm{H_2O,out}} - \delta D_{\mathrm{in}} \chi_{\mathrm{H_2O,in}}}{\chi_{\mathrm{H_2O,out}} - \chi_{\mathrm{H_2O,in}}} \quad (11)$$

Here, $\chi_{\mathrm{H_2O}}$ is the mole fraction of water vapour in dry air; "in" refers to air entering the chamber and "out" refers to the well-mixed air leaving the chamber.

3.2.2. Branch enclosures

Branch enclosures were installed to allow measurement of δD in transpirate ($\delta D_{\mathrm{trans}}$). The purpose of this was to produce a time series of daily flux-weighted values of $\delta D_{\mathrm{trans}}$ as estimates of δD in xylem ($\delta D_{\mathrm{xylem}}$), for use as input to the leaf component of the isotopically enabled SVAT model. Each branch enclosure consisted of a shaded 12.5 L transparent polyethylene cylinder with a fan, an inlet tube and an outlet tube. Pairs of branch enclosures, one empty reference enclosure and one enclosure containing a small branch, were installed at 1.5 m height in a young sapling and at 20 m height in a mature tree. Each enclosure was flushed continuously at 3 L min^{-1} with ambient air. At two-hourly intervals, air from the outlet tubes of the reference and sample enclosures was sampled sequentially by the FTIR. This allowed the δD of the transpirate in the branch enclosure to be computed using Eq. (11), with "in" referring to air from the reference enclosure and "out" referring to air from the sample enclosure. The reference enclosure was used to insure that the "in" and "out" air streams were subjected to the same buffering volume.

3.2.3. Leaf and xylem water

Deuterium contents of leaf and xylem water were measured for the purpose of testing in isolation the leaf component of the isotopically enabled SVAT model. Measured $\delta D_{\mathrm{xylem}}$ was also used to initialise the δD profile of the modelled soil water. Triplicate leaf samples were collected from saplings at three-hourly intervals during the leaf-level gas-exchange measurement period (midday 16 November (doy 320)–midday 18 November (doy 322) 2006). Traces of the leaves' outlines were recorded to determine leaf area. The leaves were then picked, folded and stored frozen in gas-tight collection vials. Simultaneously, triplicate samples of sapling xylem were similarly stored. Less frequent samples of xylem from a mature tree (the same tree as that on which the branch enclosures were installed) were also obtained. Tissue water was extracted from leaves and xylem by vacuum distillation. Leaf water volume was determined and δD of the water samples was measured using a continuous-flow isotope ratio mass spectrometer (Isoprime, Micromass, Middlewich, UK). Xylem water fraction of bulk leaf water was determined from separate leaf samples.

3.2.4. Leaf-level gas-exchange

Before leaves were picked for isotopic analysis, exchanges of water vapour and CO_2 were measured for each leaf sampled using a LiCor 6400 (LiCor, Lincoln, NE). The purpose of this was to obtain day and night time series of stomatal conductance and leaf temperature for use in validating the leaf-level model for the isotopic composition of leaf water (and hence transpirate) against observations.

4. Modelled source/sink distributions

In this section we briefly review the SVAT model, which was also used in Hav09, before describing extensions to enable prediction of δD in soil evaporate and transpirate (δD_{evap} and $\delta D_{\mathrm{trans}}$). We then present SVAT model predictions of the ground/canopy partition for CO_2, sensible heat and latent heat, and the deuterium content of the transpirate and soil evaporate for the two-week campaign period.

4.1. SVAT model

Vertical source/sink distributions of heat, water vapour and CO_2 were predicted using a multi-layered canopy model originally developed by Leuning et al. (1995), with improvements described by Wang and Leuning (1998) and Haverd et al. (2007). The core of the model is a leaf-level sub-model that couples stomatal conductance, photosynthesis and energy partitioning in response to radiation absorption, temperature and water vapour pressure deficit at leaf surfaces. Four key parameters in the sub-model were estimated by minimizing a cost function of residuals between predicted and net fluxes (of H, λE and F_c) measured above the canopy.

The radiation sub-model, based on the two-stream approximations of Goudriaan and van Laar (1994), was used to calculate the rates of radiation absorption by sunlit and shaded leaves and by the soil in the visible, near-infrared and thermal wavebands. The leaf angle distribution parameter in the submodel for radiation transfer within the canopy (Sellers, 1985) was optimised independently, to minimize the residuals between model estimates and measurements of P_{gap} (Jupp et al., 2009), the probability of a direct beam not intercepting vegetation, at a range of view angles and heights. The mean vertical leaf area density profile, that was obtained by Jupp et al. (2009) from P_{gap} using in-canopy Lidar measurements, was a direct input to the model, as were local hourly meteorological data, and local hourly measured vertical profiles of air temperature, water vapour and CO_2 concentrations.

Respiration rates of soil and vegetation were calculated using functional relationships between respiration and soil and air temperatures obtained from chamber measurements (Keith and Wong, 2006).

Fluxes of sensible and latent heat at the soil surface were calculated using a soil model called Soil–Litter–Iso (Haverd and Cuntz, 2010). This is an extension of the one-dimensional model for coupled transport of heat and water in soil and litter (used in Hav09) to include coupled transport of stable isotopes (HDO and $H_2{}^{18}O$).

4.2. Isotopically enabled soil model

Soil–Litter–Iso is a one-dimensional model for coupled transport of heat, water and stable isotopes (HDO and $H_2{}^{18}O$) in soil and litter. Given inputs of net radiation absorption, water uptake by roots and below-canopy meteorological forcing (precipitation, wind speed, air temperature), it produces estimates of vertically resolved fluxes and stores of heat, soil moisture and the minor stable isotopologues of water. The model includes the complexity of coupled heat and water transport, enabling decomposition of the total moisture flux into liquid and vapour components. Resolution of the vapour phase is particularly important for predicting steep near-surface gradients in the concentration profiles of the minor isotopic species, which in turn strongly influence the isotopic content of the evaporative flux. The numerical implementation is based Ross' fast solution to the Richards equation (Ross, 2003). It also incorporates explicit solution of the energy and moisture conservation equations at the soil/air interface, enabling resolution of temperature, humidity and isotopologue concentration at the interface (as distinct from the bulk quantities in the top soil layer).

4.3. Isotopically enabled leaf model

Estimates of the deuterium content of the transpirate were obtained using an advection–diffusion model for transport of water isotopes in leaves (Cuntz et al., 2007). This calculates the isotopic gradient between leaf incoming xylem water and water at the evaporating site using leaf characteristics and boundary conditions, i.e. the meteorologic and isotopic environment. Leaf characteristics are, for example, the asymmetry between abaxial and adaxial mesophyll cell volume, which were derived from the literature (James and Bell, 2001). Environment variables include atmospheric relative humidity but also the isotopic composition of water vapour, for example. In contrast to Cuntz et al. (2007), we used kinetic fractionation factors of Merlivat (1978) that were confirmed by Luz et al. (2009).

The leaf characteristic length for water diffusion L_{eff}, was fitted against bulk leaf water observations of δD (Section 4.4.2). This effective length was then used for calculation of δD of the transpirate at each canopy level. The model also requires the δD of xylem water, which was estimated from a combination of measurements of transpirate in branch enclosures and xylem samples (see Section 4.5). Atmospheric conditions (H_2O and HDO concentrations, air temperature) were measured and stomatal conductance and leaf temperature calculated by the SVAT model.

4.4. Validation of soil and leaf isotopic components of SVAT model

Here we validate the predictions of δD_{evap} and δD_{trans} from the soil and leaf models using measurements of δD in soil chamber evaporate and leaf water respectively. The soil model requires as input an initial vertical profile of δD of soil water. For this we assume a uniform value corresponding to that of the xylem water (δD_{xylem}) at the start of the simulation period (doy 322). The leaf model also uses the measured value of δD_{xylem}, both as an initial estimate of the deuterium content of the leaf water, and as the value for xylem water in the model (which was assumed constant over the two-day validation period). Error-weighted combination of measurements of δD in xylem water from sapling and mature tree samples on doy 322 led to a value of -46.5 ± 5‰.

4.4.1. Validation of predictions of δD in soil evaporate

Fig. 1(i) shows δD_{evap} inside the soil chamber over a ten-day measurement period. Air temperature was not measured, but estimated via a chamber surface energy balance, knowing the radiation flux at the chamber surface and the air flow rate through the chamber, and assuming no change in heat storage and an albedo of 0.7. Another unknown was the resistance between the soil surface and the bulk flow in the chamber, largely influenced by the fan on the roof of the chamber. We adjusted this parameter to a value of $3\ m^{-1}$ s, which optimised agreement between modelled and observed latent heat fluxes. In spite of these approximations, the major features of the measured time series of δD_{evap} are well captured by the model. In particular the magnitude of the rise in δD_{evap} over the first three days, corresponding to the first phase of drying, is well simulated. Also, the magnitudes of the diurnal variations, resulting from fluctuating relative humidity, are well reproduced by the model. Finally, the absolute values of the observations and predictions are in good agreement, justifying our choice of initial δD profile in the soil water.

4.4.2. Validation of predictions of δD in leaf water (and hence transpirate)

We used the measurements of δD in xylem water for doy 322 of -46.5 ± 5 ‰ together with leaf-level gas exchange (Section 3.2.4) and the FTIR spectrometer measurements of atmospheric δD to model the isotopic composition of mesophyll water. Further

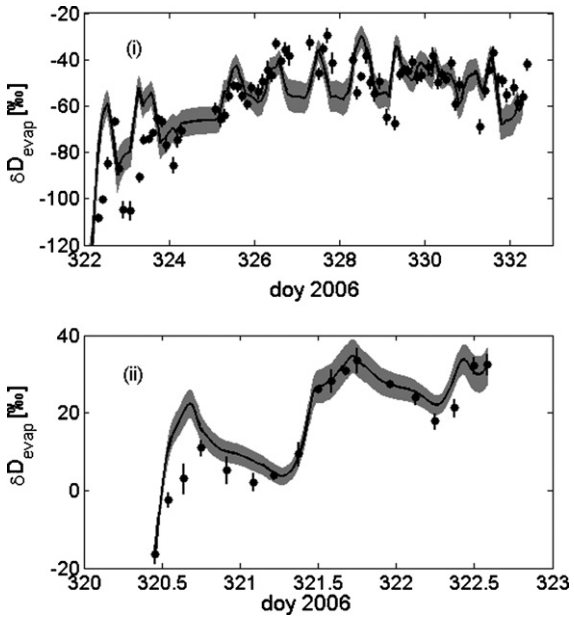

Fig. 1. Deuterium content of: (i) soil evaporate inside soil chamber; (ii) leaf water in sapling leaves. Symbols are observations with error bars representing one standard error. The shading for δD_{evap} represents the standard error propagated from errors in the initial estimate of δD in the soil water profile. For δD_{leaf}, the model standard error is propagated from the standard error in δD_{xylem}.

model inputs were the volumetric leaf water content determined as $10.7 \pm 0.4\ mol\ m^{-2}$ and the amount of mesophyll on bulk leaf water, estimated to be around 10% from literature leaf characteristics (James and Bell, 2001). The effective length of water diffusion in leaves was fitted by comparing modelled and measured bulk leaf water isotopes to $L_{eff} = 17$ mm. Fig. 1(ii) shows the time evolution of modelled against measured leaf water isotopes δD_{leaf}. The model captures the major features of the measurement time series. The good agreement at the end of nights reflects good accuracy in the measurements of δD in atmospheric water vapour (by FTIR) since night-time values mainly dependent on this variable. The day-time values, which depend on δD_{xylem}, atmospheric δD, humidity, L_{eff}, and gas exchange parameters, are well reproduced, except at the beginning of the simulation. Also, the overnight decrease in δD_{leaf}, which is highly dependent on night-time stomatal conductance, is well represented by the model, giving confidence in our leaf-level gas exchange measurements, especially at night, when small conductances can be difficult to measure.

4.5. SVAT model predictions of source/sink distributions

Fig. 2 shows the ground/canopy partitions for R_{net}, H, λE and CO_2. These as very similar to those presented in Hav09, with slight differences arising from modifications to the soil module. Note that the sensible and latent heat partitions are prior estimates, to be adjusted using the $x_{\lambda E}$ parameter during the optimisation of modelled vertical concentration profiles against observed ones.

We now turn to the SVAT model predictions of δD_{evap} and δD_{trans}. Fig. 3(i) (dotted line) shows the time course of δD_{xylem} used as input to the leaf level model, as well as the corrected daily branch enclosure estimates from which it is derived. Specifically, the leaf water input from the xylem was determined as the flux-weighted mean of transpired water in the branch enclosures, corrected by an offset (−6‰) to direct xylem isotope measurements. Fig. 3(ii) shows the modelled time series of δD_{evap} and δD_{trans}. δD_{trans} was modelled for each of 20 heights in the canopy, using leaf temperature and stomatal conductance at each height from the SVAT model, and

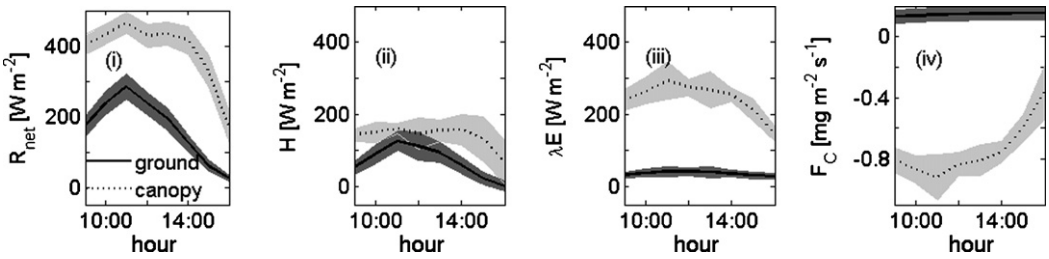

Fig. 2. Modelled ground/canopy sources, averaged over 11 clear-sky days during the period doy 322–332, 2006. (i) Net radiation absorption; (ii) sensible heat flux; (iii) latent heat flux; and (iv) CO_2 flux. Shaded areas represent standard errors on the mean, with contributions from uncertainties in the leaf area density distribution profile and net fluxes above the canopy the ground CO_2 flux.

observed vertical atmospheric profiles of δD and humidity interpolated to the same 20 heights. δD_{trans} typically increased by about 1.1‰ for sunlit and 3.5‰ for shaded leaves from the bottom to the top of the canopy around noon, and the values presented here are the flux-weighted mean values for the whole canopy. δD_{trans} exhibits an increase over the first four days of the simulation, corresponding to the increase in δD_{xylem} over the same period. The diurnal variations result from non-steady state effects and hence in day-time values of δD_{trans} that are slightly higher and night-time values that are slightly lower than δD_{xylem}. δD_{evap} shows a much steeper rise in the first four days, and this is because, during the first phase of drying, the surface soil moisture available for evaporation becomes enriched much more rapidly than the xylem water. While the isotopic model output are presented as δD, we used model predictions of the HDO source distribution for modelling the atmospheric HDO concentration profile via Eq. (2), with subsequent conversion to δD for optimisation against observations.

Isotopic disequilibrium between the evaporation and transpiration components is a necessary condition for deuterium content of water vapour to provide additional constraint on the partition of *ET*. At doy 327, the night-time values of δD_{evap} and δD_{trans} approach each other, but there is still a strong disequilibrium between the daytime values. The strong day-time disequilibrium is further illustrated by Fig. 3(iii). Here hourly ensemble values of δD_{evap} and δD_{trans} have been constructed by detrending (subtracting the daily mean from) the hourly values, taking ensemble averages over each hour of day and then adding the mean value for the whole time series. Again, the results indicate a significant disequilibrium between δD_{evap} and δD_{trans}. We also see here a strong increase of δD_{evap} during the day and a slight decrease in δD_{trans}. Flux-weighted mean values of δD_{evap} and δD_{trans} for the period doy 322–332 reveal a 24‰ disequilibrium between the components of the mean water vapour flux.

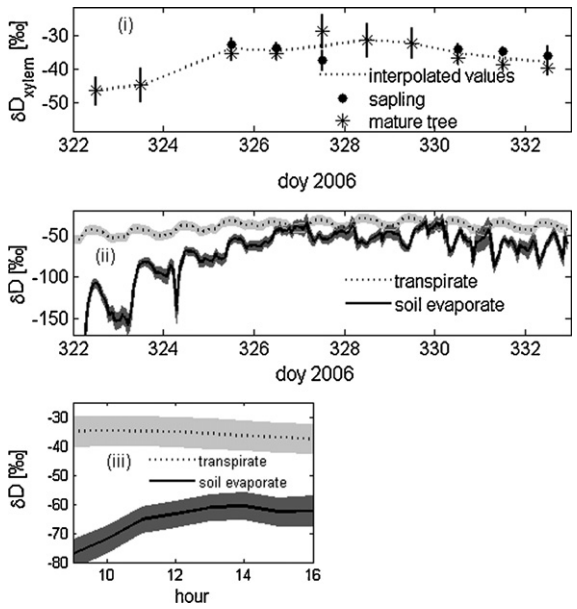

Fig. 3. δD content of (i) xylem; (ii) modelled soil evaporate; and (iii) modelled transpirate. Xylem values are interpolated from flux-weighted measurements of δD in transpirate from two branch enclosures. Shading represents standard errors, as in Fig. 1.

Historically, most isotope-based separations of transpiration and evaporation (Ferretti et al., 2003; Moreira et al., 1997; Williams et al., 2004; Xu et al., 2008; Yakir and Wang, 1996; Yepez et al., 2005) have relied on much simpler estimates of the isotopic content of the soil evaporate. These involve applying the Craig and Gordon equation (Craig and Gordon, 1965) (which accounts for equilibrium and diffusive fractionation effects), assuming the isotopic content of the liquid water is that of the soil moisture in the top few cm of soil, or at the evaporating front, or integrated over the soil column. We estimated δD_{evap} by this method, using δD of liquid water from the modelled soil moisture profiles. The results deviated from those in Fig. 3(ii) by at least 70‰. This highlights a large source of uncertainty associated with estimating the isotopic content of the soil evaporate using the isotopic composition of water extracted from soil samples.

5. Results and discussion

Fig. 4 shows the hourly ensemble mean modelled and measured vertical profiles of potential temperature, water vapour. δD in water vapour and CO_2, referenced to their values at the top of the canopy (40 m). Model profiles were generated using optimised parameters c_1, c_2 (Eq. (6)) and $x_{\lambda E}$. Black and light shaded grey areas correspond to model predictions generated using parameters optimised with cost functions constructed with $n = \{\theta, H_2O, CO_2\}$ and $v = \{\theta, H_2O, CO_2, \delta D\}$ respectively. Overlap between the two sets of model predictions is represented by dark grey shading.

As in Hav09, the non-isotopic species are well simulated with $v = \{\theta, H_2O, CO_2\}$. However, the parameters which optimise the agreement between modelled and measured non-isotopic profiles, produce modelled δD profiles which significantly underestimate the increase of δD near the ground. When δD also contributes to the cost function: i.e. $v = \{\theta, H_2O, CO_2, \delta D\}$, model/measurement overlap for δD is much improved, while the predictions for the non-isotopic profiles overlap with the simulations which do not utilise δD information. The fitted parameters corresponding to the model predictions in Fig. 4 are given in Table 1, and the corresponding vertical profiles of T_L are shown in Fig. 5. Upon inclusion of δD in the cost function, the T_L profile shifts to lower values which are closer to the prior estimate and also closer to earlier theoretical estimates (see Hav09 and references therein) of T_L at the top of the canopy. The value of the normalised T_L at the top of the canopy in Fig. 5(i) (0.51 ± 0.1) is lower than that reported in Hav09 (0.66 ± 0.1). This difference is largely attributable to different weighting coefficients

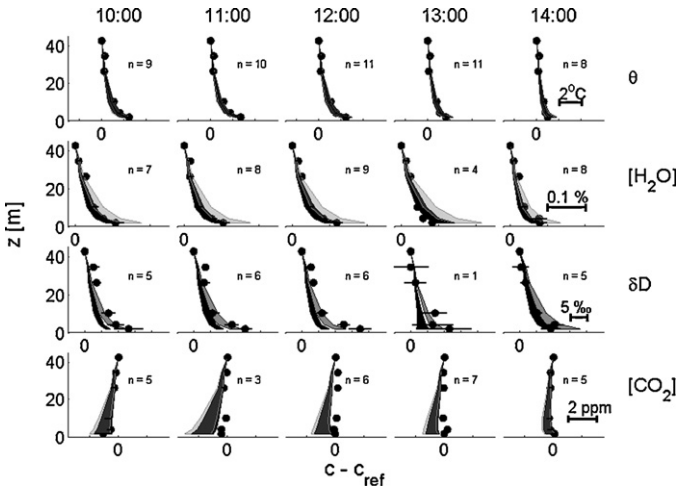

Fig. 4. Mean measured profiles (dots) and corresponding predicted vertical profiles of potential temperature, water vapour, δD of water vapour, and CO_2 concentration. Predictions using parameters obtained with $\nu = \{\theta, H_2O, CO_2\}$ are in black; predictions using parameters obtained with $\nu = \{\theta, H_2O, CO_2, \delta D\}$ are in light grey. Overlapping predictions are in dark grey. The shaded areas represent standard error bounds on model profile predictions, with errors propagated from standard errors in the modelled vertical source distributions.

Table 1
Optimised parameter values for coefficients in the T_L parameterisation and the parameter for adjusting the latent heat flux at the soil.

	Prior	Optimised (no δD)	Optimised (δD included)
c_1	7.32	6.6 ± 3	7.1 ± 2
c_2	0.32	0.51 ± 0.1	0.41 ± 0.1
$x_{\lambda E}$	0.0	0.09 ± 0.06	−0.02 ± 0.07

for the two studies: in this work we constructed the cost function such that each species contributes equally to the prior cost, whereas in Hav09, each profile point was weighted according to model and measurement uncertainty. The high sensitivity of estimated parameters to cost function formulation is discussed in detail by Trudinger et al. (2007).

Qualitatively, T_L is a measure of the persistence of the turbulence. Thus it is expected that lower values (corresponding to less efficient mixing) be required to match the steep gradients seen in the observed δD profiles. A corresponding over-prediction of the gradient in the water vapour profiles is avoided by adjusting $x_{\lambda E}$ such that the latent heat flux at the ground is lower by 2% than the prior estimate. In contrast, in the case without δD in the cost function, $x_{\lambda E}$ was adjusted such that the latent heat flux at the ground is higher than the prior value by 9%. The corresponding partitions of *ET* are given in Table 2, alongside the prior estimate. Uncertainty estimates are standard errors, propagated from uncertainties in source/sink distributions. Optimised values are revised estimates, obtained by multiplying the prior estimate by optimised $(1 + x_{\lambda E})$.

The values in Table 2 indicate that, in spite of very different δD profile predictions, the two optimised parameter sets yield partitions of *ET* which are indistinguishable within error bounds. The T_L profiles resulting from the two cases are also indistinguishable within uncertainty limits, although the case which utilises δD information yields slightly smaller uncertainty estimates. The reduction in uncertainty can be seen by comparing the shaded areas on the T_L profiles in Fig. 5(i) and (ii).

It is clear from the results presented above that both the partition of *ET* and the vertical profile of T_L are quite insensitive to the inclusion of δD in the parameter estimation process. Two possible reasons for this are suggested and investigated below.

The first possibility is that the other species already tightly constrain the parameters, such that there is little more to be gained by including the additional δD information. First, we investigated this by repeating the optimisation process with $\nu = \{\delta D, H_2O\}$ in the cost function. This led to more uncertain parameter estimates: ($c_1 = 31 \pm 30$; $c_2 = 0.71 \pm 0.3$; $x_{\lambda E} = -0.38 \pm 0.54$) compared to the case with $\nu = \{\theta, H_2O, CO_2\}$ (see Table 1), indicating that the latter combination of observation types provides a relatively strong constraint. Second, we repeated the optimisation process with $\nu = \{\theta, H_2O, CO_2, \delta D\}$, this time with a 70‰ perturbation to δD_{evap}, consistent with errors associated with traditional approaches to estimating δD_{evap}, as discussed in Section 4.5. Surprisingly, even with this large perturbation to our estimate of δD_{evap}, we were still able to produce predicted profiles of all species which overlapped measurements within standard error bounds, and the parame-

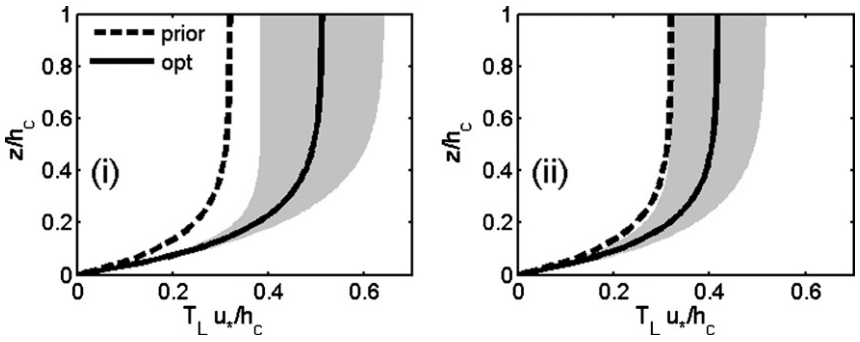

Fig. 5. Prior and optimised estimates of T_L: (i) without including δD in cost function, $\nu = \{\theta, H_2O, CO_2\}$; (ii) including δD in cost function, $\nu = \{\theta, H_2O, CO_2, \delta D\}$. Shaded areas represent standard errors, which arise from uncertainties in the vertical source/sink distributions and uncertainties in the retrieved parameters (c_1 and c_2 in Eq. (1)) for a given source/sink distribution.

Table 2
Ground/canopy latent heat flux partition and ratio of transpiration to total latent heat flux: mean values for 11 clear-sky days during the period doy 322–332, 2006.

	λE_{prior} (MJ m^{-2} d^{-1})	λE_{opt} (no δD) (MJ m^{-2} d^{-1})	λE_{opt} (δD) (MJ m^{-2} d^{-1})
Ground	1.8 ± 0.17	2.0 ± 0.2	1.8 ± 0.2
Canopy	10.3 ± 0.5	10.1 ± 0.5	10.3 ± 0.5
Transpiration fraction	0.85 ± 0.02	0.83 ± 0.02	0.85 ± 0.02

ter estimates ($c_1 = 7.1 \pm 4$; $c_2 = 0.41 \pm 0.1$; $x_{\lambda E} = -0.03 \pm 0.03$) were close to those obtained using our unperturbed estimate of δD_{evap}. This result indicates that a large change in the isoflux at the ground can be readily compensated for by small changes in $x_{\lambda E}$ and the turbulence parameters, leaving the optimised modelled profiles little changed. These two investigations thus substantiate our first explanation, that our target parameters are well constrained by the non-isotopic observations.

The second possibility is that δD contributes only one quarter of the prior cost function. When we repeated the optimisation with $v = \{\delta D, H_2O\}$ (with δD contributing to half of the prior cost function), we found that the estimated parameters were indeed sensitive to δD being given a higher weighting, but they were also less tightly constrained and the turbulence parameter values became extreme. Thus the second possibility is substantiated, but does not suggest that weighting δD more highly achieves better results.

6. Conclusion

The modelled vertical concentration profiles resulting from inclusion of δD in the cost function demonstrate our ability to make consistent estimates of both the scalar source distributions and the deuterium content of the water vapour sources. However, introducing measurements of deuterium in water vapour does not significantly alter resulting estimates of T_L and the partition of *ET*, compared with the case when only temperature, water vapour and CO_2 concentration profiles are available. We propose a revised estimate of T_L, corresponding to that obtained using δD (see Table 1), since this result utilises all the experimental information available. The lack of significant difference between estimates of the partition of *ET* with and without δD (in spite of significant isotopic disequilibrium (ca. 24‰) between *ET* components) arises because δD only contributes to one quarter of the prior cost function and because the *ET* partition is already well constrained by the fluxes of sensible heat, CO_2 and water vapour, together with their associated measured concentration profiles and modelled source/sink distributions. The latter reason suggests that the additional data and modelling required to use deuterium are not warranted for the purpose of partitioning *ET* using the framework presented here.

Acknowledgements

We gratefully acknowledge the expert technical assistance of Steve Zegelin, Dale Hughes, Mark Kitchen, Richard Hurley, Martin Riggenbach and Graham Kettlewell. Thanks also to David Jupp for supplying the ground-based Lidar data, Heather Keith and Stephen Livesley for the ground CO_2 flux measurements and Ray Leuning and Eva van Gorsel for the turbulence measurements. Eva van Gorsel and Ray Leuning kindly reviewed the manuscript and provided helpful suggestions. This work was supported in part by a grant form the Australian Climate Change Science Program.

Appendix A. Analysis of trace gases and isotopic ratios in air by FTIR spectrometry

A.1. Introduction

Optical methods such as Fourier Transform Infrared (FTIR) or laser absorption spectrometry can be deployed in the field and used to analyse water vapour and other trace gases, including isotopologues, continuously in whole air samples. They can provide real time measurements and a much higher data density than conventional IRMS analysis, although in some cases with somewhat lower accuracy or precision per measurement.

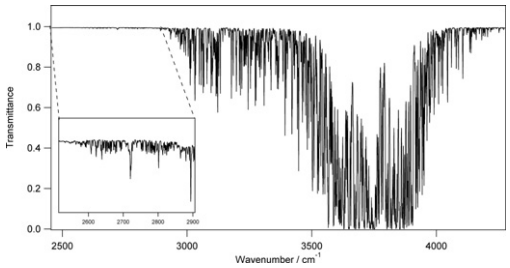

Fig. A1. Infrared transmission spectra from 2500 to 4000 cm^{-1} of H_2O (main trace) and HDO (inset trace) in natural abundance at typical atmospheric humidity.

FTIR spectroscopy measures the broad-band infrared absorption spectrum of an air sample, which can be analysed to retrieve concentrations of many compounds simultaneously. For an introduction to FTIR applications in atmospheric trace gas analysis, see reviews by Griffith (2002) and Griffith and Jamie (2000) and references therein. A more complete description and recent application to high accuracy clean air measurements is described by Griffith et al. (2010). In the case of D/H ratios in water vapour, FTIR spectroscopy measures the absolute concentrations of HDO ($^2H^1H^{16}O$) and H_2O ($^1H^1H^{16}O$) molecules directly in a whole air sample, from which the isotope ratio and δD is determined. Similarly, $\delta^{13}C$ in CO_2 is determined from measurements of the individual $^{13}CO_2$ and $^{12}CO_2$ isotopologues. The FTIR spectrometer is portable for field use, and no sample treatment is required – whole air is drawn through a sample cell and its IR spectrum is measured continuously in real time to provide the required analysis.

Due to the factor of two mass difference between D and H, the O–D stretching vibration of HDO is shifted by several hundred wavenumbers from that of O–H in H_2O, so that it (fortuitously) appears in an otherwise uncluttered region of the infrared spectrum. Fig. A1 illustrates the spectra and the regions used for H_2O and HDO analysis. The large separation between H_2O and HDO bands and lack of major interference from other molecules allows the use of a compact, low resolution spectrometer suited to field studies.

A.2. FTIR instrumentation and measurements

Air was drawn continuously at 2 L min^{-1} from each of seven inlets on the tower at 2.0, 4.4, 10.4, 26.3, 35.4, 43.4, 70.1 m with a small membrane pump through identical lengths of 9.25 mm OD Dekabon^{TM} tubing. All lines were heated up to the 40 m level to avoid condensation of water vapour in cold conditions near the ground. In each 30 min measurement cycle, air from each of the seven inlet lines was analysed sequentially to provide one seven-point vertical profile, allowing 250 s for each inlet line measurement. Within each 250 s sample period, the spectrometer cell was rapidly evacuated (4-stage membrane pump, Brand MV2) and re-filled from the next inlet line to be analysed. A steady flow of 2 L min^{-1} from the inlet line and cell was then established and the FTIR spectrum recorded for the last 120 s of the 250 s period. The

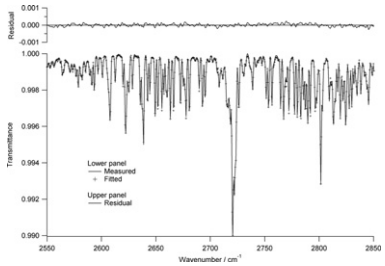

Fig. A2. Example of a spectral fit in the HDO fitting region. In the lower plot the solid line is the measured spectrum and the crosses are the fitted spectrum. The upper trace is the difference between measured and fitted spectra.

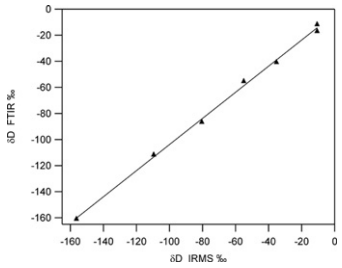

Fig. A3. Calibration of FTIR measurement of δD on 10 November 2006. *X* axis: δD values of reference water samples determined by IRMS. *Y* axis: FTIR measurements. The regression equation is $y = 1.001x - 3.26$ and standard error of prediction is 2.7‰.

analysis of each spectrum to provide component concentrations and δD values was performed in real time (as described below) at the end of each 250 s sample period. All valve switching, pressure and temperature measurements, spectrometer operation and spectrum analysis were carried out automatically under control of a single Visual Basic program running on a laptop PC. Results were displayed in real time and could be downloaded at any time for further analysis on a separate PC.

Two FTIR analysers were employed; in one the airstream was flowed undried through the sample cell for water vapour and δD analysis, in the other the air stream was dried by a Nafion® membrane drier (Permapure PD-100T24MSS, NJ, USA) and magnesium perchlorate trap for more accurate analysis of other trace gases.

The FTIR spectra were recorded from 2000 to 5000 cm^{-1} at 1 cm^{-1} resolution with Bruker IRcube FTIR spectrometers (Bruker Optics, Ettlingen, Germany) fitted with TE-cooled, mercury cadmium telluride (MCT) detectors (J19TE3, 5 μm cutoff, Judson Technologies, PA, USA) to obtain a high signal:noise ratio, and with 26 m multipass White cells (model PA26, volume 3.5 L, Infrared Analysis Inc. CA, USA) to enhance the IR absorption of HDO (Fig. A1). The spectrometer and cell were thermostatted to 34 °C to ensure stability and avoid temperature-dependent calibration fluctuations. The IR beam path through the spectrometer and outside the sample cell was purged with nitrogen to remove interference from CO_2 and water vapour outside the sample cell. The spectrometers and sampling system operated continuously and automatically for the entire period of the campaign.

A.3. Spectrum analysis

Spectra were analysed by a non-linear least squares fitting technique, in which the measured FTIR spectrum is fitted with an iteratively calculated spectrum until a least-squares best fit is obtained. The concentrations of absorbing molecular species were determined from the values which achieve best fit to the measured spectrum. For further details see (Feilberg et al., 2002; Griffith, 1996). In the spectral region 2000–5000 cm^{-1} collected by the spectrometer, HDO was fitted in the region 2600–2840 cm^{-1}, H_2O and CH_4 from 2940 to 3156 cm^{-1} (see Fig. A1), and CO_2, CO and N_2O from 2102 to 2320 cm^{-1}. An example of a fitted spectrum in the HDO region is shown in Fig. A2, which displays the measured, fitted and residual spectra. The calculation is sufficiently accurate to fit the measured spectrum to close to its noise level.

A.4. Calibration

The least squares fitting procedure used for quantitative spectrum analysis is based on tabulated spectral data (HITRAN 2004; Rothman et al., 2005) and requires no calibration gases; it provides a working calibration for trace gas concentrations and δD which is usually accurate to better than 5% and precise to ca. 0.1% for H_2O, HDO, CO_2, CH_4 and N_2O at ambient levels (Esler et al., 2000; Griffith, 1996). For more accurate absolute calibration, measurements must be compared to independently calibrated reference gases. For CO_2, CH_4 and N_2O, measurements of two reference tanks of air calibrated in CSIRO's GASLAB were performed in the field before, during and after the campaign period. The calibration drifts were less than 1% over the 16-day duration of the campaign and a time-dependent calibration factor was applied to all data to bring them to the common calibration scale.

For water vapour mixing ratios, the difficulty of introducing air with accurately known water vapour concentrations into the measurement cell, and adsorption and memory effects of cell and tubing walls, precluded calibration under field conditions. We therefore rely on the spectral fitting alone for calibration with uncertainty estimated to be at most 5% as described above (see also Smith et al., 2010). In the previous work we demonstrated this level of accuracy in a similar measurement situation by comparison of FTIR measurements of water vapour on a 22 m tower with Vaisala Humitter sensors (Griffith et al., 2002). In the present work, we have compared the FTIR measurements of water vapour with those from an infrared gas analyser (LI6262, Licor Inc., Lincoln, Nebraska) which sampled air from the same heights on the tower. These comparisons are consistent with the quoted 5% accuracy for the FTIR measurements.

Calibration for δD in water vapour presents a more difficult challenge, since calibrated isotopic reference water samples are available as liquid water but the FTIR analysis is fundamentally a vapour measurement. To calibrate for δD, we measured the FTIR spectra of up to ten liquid water samples of known δD (V-SMOW) analysed by isotope ratio mass spectrometry at CSIRO Land and Water, Adelaide. The liquid samples were quantitatively vapourised into a continuous flow of 2–4 L min^{-1} dry air from a high pressure tank in a heated block at 120 °C to provide mixing ratios typical of the air samples to be measured – 0.5–1.5 mol%. Each reference water sample flowed through the spectrometer cell until the real-time-indicated δD was steady, typically 25–30 min per sample. Raw FTIR measurements were corrected for a small dependence on the absolute water vapour concentration. A typical calibration of FTIR vs IRMS is shown in Fig. A3. Calibration was performed before, during and after the campaign. The standard error of prediction from the regressions is typically 1–3‰ for 2 min measurements of δD, and FTIR values of δD in this work have analytical precision of this order. Wall memory effects in the cell and tubing which differ between H_2O and HDO molecules may add further uncertainty in accuracy which we estimate to be of the same order.

References

Allison, G.B., Barnes, C.J., 1983. Estimation of evaporation from non-vegetated surfaces using natural deuterium. Nature 301 (5896), 143–145.

Craig, H., Gordon, L.I., 1965. Deuterium and oxygen-18 variations in the ocean and the marine atmosphere. In: Tongiorgi, E. (Ed.), Proceedings of a Conference on Stable Isotopes in Oceanographic Studies and Paleotemperatures Spoleto. Italy, Consiglio Nazional delle Richerche, Pisa, pp. 9–130.

Cuntz, M., Ogee, J., Farquhar, G.D., Peylin, P., Cernusak, L.A., 2007. Modelling advection and diffusion of water isotopologues in leaves. Plant Cell and Environment 30 (8), 892–909.
Doherty, J., 1999. PEST. Watermark Numerical Computing, Townesville.
Esler, M.B., Griffith, D.W.T., Wilson, S.R., Steele, L.P., 2000. Precision trace gas analysis by FT-IR spectroscopy 1. Simultaneous analysis of CO_2, CH_4, N_2O and CO in air. Analytical Chemistry 72 (1), 206–215.
Evans, J.R., Sharkey, T.D., Berry, J.A., Farquhar, G.D., 1986. Carbon isotope discrimination measured concurrently with gas exchange to investigate CO_2 diffusion in leaves of higher plants. Australian Journal of Plant Physiology 13, 281–292.
Farquhar, G.D., Lloyd, J., Taylor, J.A., Flanagan, L.B., Syvertsen, J.P., Hubick, K.T., Chin Wong, S., Ehleringer, J.R., 1993. Vegetation effects on the isotope composition of oxygen in atmospheric CO_2. Nature 363 (6428), 439–443.
Feilberg, K.L., Sellevag, S.R., Nielsen, C.J., Griffith, D.W.T., Johnson, M.S., 2002. $CO + OH \rightarrow CO_2 + H$: the relative reaction rate of five CO isotopologues. Physical Chemistry Chemical Physics 4 (19), 4687–4693.
Ferretti, D.F., Pendall, E., Morgan, J.A., Nelson, J.A., LeCain, D., Mosier, A.R., 2003. Partitioning evapotranspiration fluxes from a Colorado grassland using stable isotopes: seasonal variations and ecosystem implications of elevated atmospheric CO_2. Plant and Soil 254 (2), 291–303.
Fest, B.J., Livesley, S.J., Drosler, M., van Gorsel, E., Arndt, S.K., 2009. Soil-atmosphere greenhouse gas exchange in a cool, temperate Eucalyptus delegatensis forest in south-eastern Australia. Agricultural and Forest Meteorology 149 (3–4), 393–406.
Gonfiantini, R., 1978. Standards for stable isotope measurements in natural compounds. Nature 271 (5645), 534–536.
Goudriaan, J., van Laar, H.H., 1994. Modelling Potential Crop Growth Processes. Current Issues in Production Ecology, 2. Kluwer Academic Publishers, Dordrecht, 238 pp.
Griffith, D.W.T., 1996. Synthetic calibration and quantitative analysis of gas-phase FT-IR spectra. Applied Spectroscopy 50 (1), 59–70.
Griffith, D.W.T., 2002. FTIR measurements of atmospheric trace gases and their fluxes. In: Chalmers, J.M., Griffiths, P.R. (Eds.), Handbook of Vibrational Spectroscopy. John Wiley & Sons, pp. 2823–2841.
Griffith, D.W.T., Deutscher, N., Krummel, P., Frase, P., Steele, P., van der Schoot, M., Allison, C., 2010. The UoW FTIR trace gas analyser: comparison with LoFlo, AGAGE and tank measurements at CApe Grim and GASLAB. In: Krummel, P., Derek, N. (Eds.), Baseline Atmopsheric Program (Australia) 2007–2008. CSIRO, Melbourne.
Griffith, D.W.T., Jamie, I.M., 2000. FTIR spectrometry in atmospheric and trace gas analysis. In: Meyers, R.A. (Ed.), Encyclopedia of Analytical Chemistry. Wiley, pp. 1979–2007.
Griffith, D.W.T., Leuning, R., Denmead, O.T., Jamie, I.M., 2002. Air-land exchanges of CO_2, CH_4 and N_2O measured by FTIR spectrometry and micrometeorological techniques. Atmospheric Environment 36 (11), 1833–1842.
Haverd, V., Cuntz, M., 2010. Soil–Litter–Iso: A one-dimensional model for coupled transport of heat, water and stable isotopes in soil with a litter layer and root extraction. Journal of Hydrology 388 (3–4), 438–455.
Haverd, V., Cuntz, M., Leuning, R., Keith, H., 2007. Air and biomass heat storage fluxes in a forest canopy: calculation within a soil vegetation atmosphere transfer model. Agricultural and Forest Meteorology 147, 125–139.
Haverd, V., Leuning, R., Griffith, D.W.T., Van Gorsel, E., Cuntz, M., 2009. The turbulent lagrangian time scale in forest canopies constrained by fluxes, concentrations and source distributions. Boundary-Layer Meteorology 130, 209–228.
Herbst, M., Kappen, L., Thamm, F., Vaneslow, R., 1996. Simultaneous measurements of transpiration, soil evaporation and total evaporation in a maize field in northern Germany. Journal of Experimental Botany 47 (305), 1957–1962.
James, S.A., Bell, D.T., 2001. Leaf morphological and anatomical characteristics of heteroblastic Eucalyptus globulus ssp globulus (Myrtaceae). Australian Journal of Botany 49 (2), 259–269.
Jupp, D.L.B., Culvenor, D.S., Lovell, J.L., Newnham, G.J., Strahler, A.H., Woodcock, C.E., 2009. Estimating forest LAI profiles and structural parameters using a ground based laser called "Echidna®". Tree Physiology 29 (2), 171–181.
Keith, H., Wong, S.C., 2006. Measurement of soil CO_2 efflux using soda lime absorption: both quantitative and reliable. Soil Biology & Biochemistry 38 (5), 1121–1131.
Leuning, R., Cleugh, H.A., Zegelin, S.J., Hughes, D., 2005. Carbon and water fluxes over a temperate Eucalyptus forest and a tropical wet/dry savanna in Australia: measurements and comparison with MODIS remote sensing estimates. Agricultural and Forest Meteorology 129 (3–4), 151–173.
Leuning, R., Kelliher, F.M., Depury, D.G.G., Schulze, E.D., 1995. Leaf nitrogen, photosynthesis, conductance and transpiration: scaling from leaves to canopies. Plant Cell and Environment 18 (10), 1183–1200.
Luz, B., Barkan, E., Yam, R., Shemesh, A., 2009. Fractionation of oxygen and hydrogen isotopes in evaporating water. Geochimica Et Cosmochimica Acta 73 (22), 6697–6703.
Merlivat, L., 1978. Dependence of bulk evaporation coefficients on air–water interfacial conditions as determined by isotopic method. Journal of Geophysical Research-Oceans and Atmospheres 83 (NC6), 2977–2980.
Moreira, M.Z., Sternberg, L.D.L., Martinelli, L.A., Victoria, R.L., Barbosa, E.M., Bonates, L.C.M., Nepstad, D.C., 1997. Contribution of transpiration to forest ambient vapour based on isotopic measurements. Global Change Biology 3 (5), 439–450.
Raupach, M.R., 1989a. Applying Lagrangian fluid-mechanics to infer scalar source distributions from concentration profiles in plant canopies. Agricultural and Forest Meteorology 47 (2–4), 85–108.
Raupach, M.R., 1989b. A practical lagrangian method for relating scalar concentrations to source distributions in vegetation canopies. Quarterly Journal of the Royal Meteorological Society 115 (487), 609–632.
Ross, P.J., 2003. Modeling soil water and solute transport – Fast, simplified numerical solutions. Agronomy Journal 95 (6), 1352–1361.
Rothman, L.S., Jacquemart, D., Barbe, A., Benner, D.C., Birk, M., Brown, L.R., Carleer, M.R., Chackerian, C., Chance, K., Coudert, L.H., Dana, V., Devi, V.M., Flaud, J.M., Gamache, R.R., Goldman, A., Hartmann, J.M., Jucks, K.W., Maki, A.G., Mandin, J.Y., Massie, S.T., Orphal, J., Perrin, A., Rinsland, C.P., Smith, M.A.H., Tennyson, J., Tolchenov, R.N., Toth, R.A., Vander Auwera, J., Varanasi, P., Wagner, G., 2005. The HITRAN 2004 molecular spectroscopic database. Journal of Quantitative Spectroscopy & Radiative Transfer 96 (2), 139–204.
Sellers, P.J., 1985. Canopy reflectance, photosynthesis and transpiration. International Journal of Remote Sensing 6, 1335–1372.
Smith, T.E.L., Wooster, J., Tattaris, M., Griffith, D.W.T., 2010. Absolute accuracy evaluation and sensitivity analysis of OP-FTIR NLS retrievals of CO_2, CH_4 and CO over concentrations ranging from those of ambient atmospheres to highly polluted plumes. Atmospheric Measurement Technical Discusssions 3, 3675–3723.
Styles, J.M., Raupach, M.R., Farquhar, G.D., Kolle, O., Lawton, K.A., Brand, W.A., Werner, R.A., Jordan, A., Schulze, E.D., Shibistova, O., Lloyd, J., 2002. Soil and canopy CO_2, (CO_2)-C-13, H_2O and sensible heat flux partitions in a forest canopy inferred from concentration measurements. Tellus Series B-Chemical and Physical Meteorology 54 (5), 655–676.
Trudinger, C.M., Raupach, M.R., Rayner, P.J., Kattge, J., Liu, Q., Pak, B., Reichstein, M., Renzullo, L., Richardson, A.D., Roxburgh, S.H., Styles, J., Wang, Y.P., Briggs, P., Barrett, D., Nikolova, S., 2007. OptIC Project: an intercomparison of optimization techniques for parameter estimation in terrestrial biogeochemical models. Journal of Geophysical Research-Biogeosciences 112 (G2).
Wang, Y.P., Leuning, R., 1998. A two-leaf model for canopy conductance, photosynthesis and partitioning of available energy I: Model description and comparison with a multi-layered model. Agricultural and Forest Meteorology 91 (1–2), 89–111.
Williams, D.G., Cable, W., Hultine, K., Hoedjes, J.C.B., Yepez, E.A., Simonneaux, V., Er-Raki, S., Boulet, G., de Bruin, H.A.R., Chehbouni, A., Hartogensis, O.K., Timouk, F., 2004. Evapotranspiration components determined by stable isotope, sap flow and eddy covariance techniques. Agricultural and Forest Meteorology 125 (3–4), 241–258.
Xu, Z., Yang, H.B., Liu, F.D., An, S.Q., Cui, J., Wang, Z.S., Liu, S.R., 2008. Partitioning evapotranspiration flux components in a subalpine shrubland based on stable isotopic measurements. Botanical Studies 49 (4), 351–361.
Yakir, D., Sternberg, L.D.L., 2000. The use of stable isotopes to study ecosystem gas exchange. Oecologia 123 (3), 297–311.
Yakir, D., Wang, X.F., 1996. Fluxes of CO_2 and water between terrestrial vegetation and the atmosphere estimated from isotope measurements. Nature 380 (6574), 515–517.
Yepez, E.A., Huxman, T.E., Ignace, D.D., English, N.B., Weltzin, J.F., Castellanos, A.E., Williams, D.G., 2005. Dynamics of transpiration and evaporation following a moisture pulse in semiarid grassland: a chamber-based isotope method for partitioning flux components. Agricultural and Forest Meteorology 132 (3–4), 359–376.